Disorder–order phase change of ω-(*N*-pyrrolyl)alkanethiol self-assembled monolayers on gold induced by STM scans and thermal activation

Joon Sung Lee,[ab] Young Shik Chi,[a] Jinhee Kim,[b] Wan Soo Yun[b] and Insung S. Choi*[a]

Received 7th January 2008, Accepted 13th March 2008
First published as an Advance Article on the web 14th April 2008
DOI: 10.1039/b800239h

Molecular ordering of pyrrolyl-terminated alkanethiol self-assembled monolayers (PyC_nSH SAMs) on Au(111) substrates (n = 11 or 12) was investigated by scanning tunneling microscopy (STM) and various spectroscopic methods. The SAMs, which were in a disordered state when formed at room temperature, could be ordered either globally by thermal annealing at 70 °C, or locally *via* stimulation with repetitive STM scans. The ordered phase was characterized by small domains of molecular rows formed along $\langle 11\bar{2}\rangle$ directional set with an inter-row corrugation period close to 1.44 nm, in which defects were abundant. Based on the experimental results, the molecular arrangement in the ordered PyC_nSH SAM was proposed to be a $(5\times\sqrt{3})$rect structure with a molecular deficiency $\geq 10\%$. While mechanical interactions between molecules and scanning probe tips had been pointed out as the major cause of scan-induced phase transformations in other SAM systems, electronic or electrostatic factors were thought to affect considerably the scan-induced ordering process in this SAM system. From comparison of surface molecular coverage between disordered and thermally ordered SAMs of $PyC_{12}SH$, it was inferred that the disorder could be ascribed to both kinetic and thermodynamic factors. The kinetic barrier to the ordered phase was supposed to result from strong dipole–dipole interactions among the pyrrolyl endgroups.

1. Introduction

Self-assembled monolayers (SAMs) of organic thiols on metal surfaces have been a subject of wide and intensive studies, for their potential applications in functional modifications of metal surfaces as well as in molecular electronics.[1] Much work on various aspects of organic thiol SAMs has been performed not only for practical applications, but also for tackling fundamental issues such as correlations between structures of SAMs and the corresponding molecular species. SAMs of normal alkanethiols on Au(111) have been most intensely studied as a model system of organic thiol SAMs, for their simplicity and ease of sample preparation. However, even for this simple model system, there are several unresolved issues such as identification of Au–S binding sites and possible Au surface relaxation in many structural phases identified so far.[2]

Substitution of the methyl terminal group in alkanethiols by other functional groups can alter the properties of their SAMs dramatically. The substitution opens up many practical possibilities such as applications in molecular electronics and soft lithography, as well as enhancement of tribological properties and stability.[3,4] Variation of structural phases dependent on terminal groups and alkyl linker length in endgroup-substituted alkanethiol SAM systems has also been a subject of many in-depth studies. In this research field, endgroup-substituted systems by aromatic moieties have been most widely studied, because these systems usually give a variety of well-defined structural phases that sensitively depend on packing configurations of the aromatic moieties. For example, structures of phenyl- or methylbiphenyl-terminated short alkanethiol SAMs have been known to be dependent on the alkyl linker length by STM studies.[5–7] It has also become well known that various structural phases of SAMs may exist for a single molecular species, depending on the formation conditions and post-treatments.[4,8–10] These studies have provided a fundamental insight on the correlation between SAM structures and various factors that govern the intermolecular and molecule–substrate interactions.

McCarley and Willicut have made a major contribution to studies on pyrrolyl-terminated alkanethiol (PyC_nSH) SAMs on Au(111) by reporting an electrochemical polymerization of the pyrrolyl endgroups,[11–13] which implied possible application of this system to molecular electronics and chemical surface engineering.[14] Although they proposed formation of polymerized patterns on those SAMs by scanning probe-based methods to be viable, there has not yet been a report of success. SAMs of PyC_nSH with $n \leq 10$ have been shown by the authors to have an almost fully disordered nature, with vibration mode frequencies and intensity ratios from infrared spectra of the methylene linkers in the SAMs similar to those of liquid molecules, and with a much smaller surface density of molecules ($\sim$50%) than that of close-packed alkanethiol SAMs. However, there have been disparities in characteristics of the SAM system such as surface molecular coverage and

[a] *Department of Chemistry and School of Molecular Science (BK21), KAIST, Daejeon 305-701, Korea. E-mail: ischoi@kaist.ac.kr; Fax: +82 (0)42 869 2810*
[b] *Korea Research Institute of Standards and Science (KRISS), Daejeon 305-600, Korea*

pyrrole ring orientation in later reports.[15–17] Moreover, there has not been an SPM-based study on the system with molecular or lattice resolution.[11]

In this article, we present the first scanning probe microscopy (SPM) study on the structures of PyC_nSH SAMs. It is shown that the SAMs (n = 11 or 12) formed at room temperature have a partially disordered structure, while they can transform into an ordered phase by STM scans or thermal annealing. Structural phase transformations by SPM scans or thermal activation have been reported in various molecular monolayer systems.[4,18–21] For example, there has been a report that a metastable $(2\times\sqrt{3})$rect phase of hexadecanethiol SAM was turned into a more stable $(\sqrt{3}\times\sqrt{3})R30^\circ$ phase by mechanical perturbation with an AFM tip.[20] There also has been a report of phase conversion at a low temperature of 35 K induced by STM scans between low-coverage phases of physisorbed azobenzene molecular layer on Au(111).[22] To our knowledge, however, there has been no report of phase transformation from disordered to ordered phases in any molecular SAM system.

In the scan-induced ordering of the SAMs, no odd–even effect was observed and the ordered phases of the PyC_nSH SAMs with n = 11 or 12 appeared to be alike. The ordered phase was composed of small domains of molecular rows formed along the $\langle 11\bar{2}\rangle$ directional set with an inter-row corrugation period of 1.47 ± 0.07 nm. Since a molecularly resolved STM image of the ordered phase could not be obtained from the SAMs, we used other experimental methods such as cyclic voltammetry (CV), X-ray photoelectron spectroscopy (XPS), ellipsometry, polarized infrared external reflectance spectroscopy (PIERS), and contact angle goniometry to investigate structural characteristics of the disordered and ordered phases of the SAMs. Based on the experimental results, the molecular arrangement in the SAM could be deduced to be a $(5\times\sqrt{3})$rect structure.

2. Results and discussion

2.1 The pristine SAM of $PyC_{12}SH$

The $PyC_{12}SH$ SAM formed at room temperature (RT) was in a disordered phase, characterized by 0.24-nm-deep etch pits typical of thiol SAMs on Au(111).[5,23] While molecular resolution in the STM images was mostly not achievable in this phase, some distinct features suggestive of partially ordered molecules could be observed at very scarce instances. Six protrusions in a row could be seen in the encircled area of Fig. 1. The average distance between the protrusions was measured to be ~0.48 nm, which was quite close to the next-nearest-neighbor (NNN) distance of Au atoms on unreconstructed (111) surface (0.4995 nm). This intermolecular distance of ~0.5 nm had already been shown to manifest itself in the $(\sqrt{3}\times\sqrt{3})R30^\circ$-based close-packed structures of alkanethiol SAMs,[2,18] as well as in the ordered $(\sqrt{3}\times 2\sqrt{3})R30^\circ$ structures of phenyl-terminated alkanethiol SAMs.[5] However, it is not clear whether this partial ordering would reveal a characteristic of the ordered phase, which is discussed below. We further note that the disordered RT-SAM did not show any sign of ordering after weeks of storage at RT.

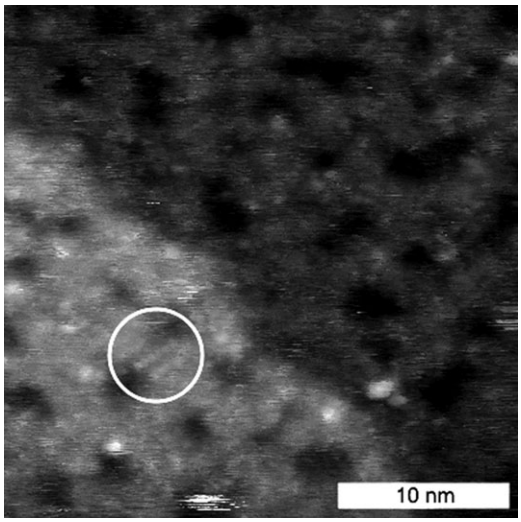

Fig. 1 An STM topograph of pristine $PyC_{12}SH$ SAM assembled at room temperature. Image was taken with I_t = 30 pA, V_{tip} = 0.5 V. The scanned area is 30 × 30 nm^2.

2.2 Scan-induced ordering of $PyC_{12}SH$ SAM

The initially disordered RT-SAM of $PyC_{12}SH$ tended to be ordered with repetitive STM scans. This scan-induced ordering was more facile with more invasive scan conditions, such as higher tunneling current setpoints or smaller tip biases. Fig. 2 shows the ordering of $PyC_{12}SH$ SAM on a Au/mica substrate by repetitive STM scans under invasive scan conditions. As is shown in Fig. 2a, the SAM was initially in a disordered phase characterized by smaller Au vacancies and fuzzy STM topography. Faint signs of partial molecular ordering could be observed already at this initial scan. After 40 min of consecutive scans, the scan-induced molecular ordering became evident (Fig. 2b). The ordering was usually accompanied by Au vacancy coarsening, or even by Au sublayer erosion.[23] The ordering efficiency—the time required for ordering of a unit area—was largely erratic, but dependent on scan conditions and tip properties to some extent.

The ordered monolayer was composed of small domains of molecular rows oriented by ~120° with respect to each other. These molecular row directions were related to three equivalent surface directions that came from the three-fold symmetry of the unreconstructed Au(111) surface. Traces of roughly triangular facets can be seen in Fig. 2a. It is well known that these facets run preferentially along $\langle 1\bar{1}0\rangle$ equivalent directions on thermally annealed Au/mica substrates.[24] Therefore, the molecular row directions corresponded to an $\langle 11\bar{2}\rangle$ equivalent set, which comprised the NNN directions on the Au(111) lattice. The domain sizes mostly did not exceed ~10 nm, and small fragments of the rows were often observed between the domains as well as in the middle of the domains. These small segments did not seem to obey the 120° rule strictly. In addition to these irregularities, other defects such as dislocations hindered an exact determination of the corrugation period of the row structure, which was observed to be close to 1.5 nm. Despite our efforts, molecular resolution of the ordered phase could not be acquired, leaving the lateral

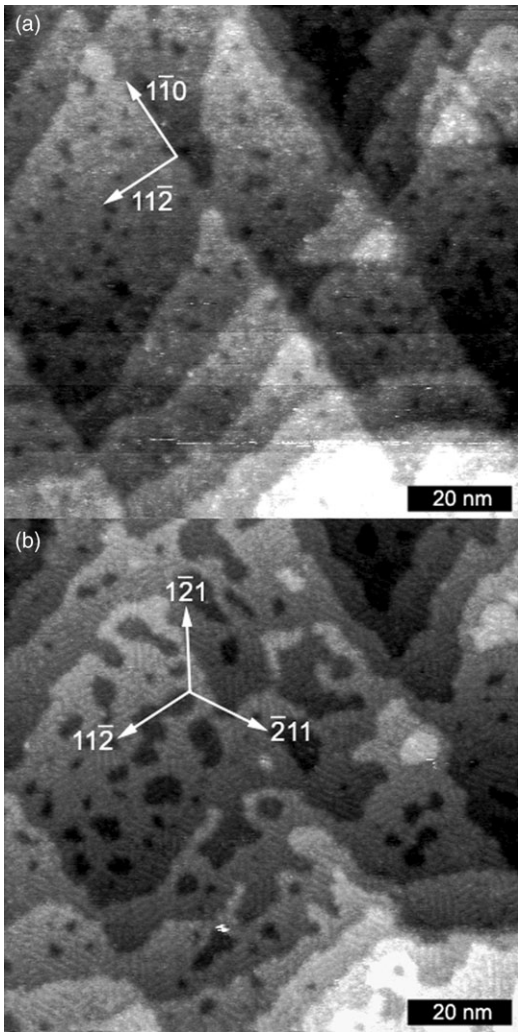

Fig. 2 STM topographs of $PyC_{12}SH$ SAM: (a) pristine RT-SAM imaged with I_t = 30 pA and V_{tip} = 0.3 V, (b) the same area imaged with I_t = 30 pA and V_{tip} = −1.0 V after 40 min of consecutive scans with the previous scan conditions. Corrugation height of the molecular rows in (b) is ~0.07 nm. The scanned area is 100 × 100 nm^2. Contrast scales are the same in both images.

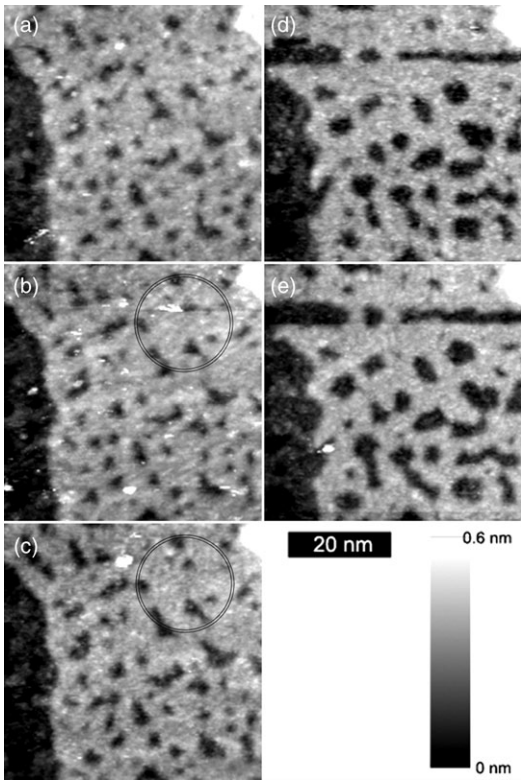

Fig. 3 STM topographs of the $PyC_{12}SH$ SAM showing dynamic pattern evolutions: (a) obtained after 20 min of scans with I_t = 50 pA and V_{tip} = −0.8 V, (b) with I_t = 500 pA and V_{tip} = 1.0 V after (a), (c) after 10 min of scans with I_t = 50 pA and V_{tip} = −0.8 V, (d) after 12 h of (c) with I_t = 50 pA and V_{tip} = −0.8 V, (e) with I_t = 500 pA and V_{tip} = −1.0 V after a scan with I_t = 500 pA and V_{tip} = 1.0 V. The selected area is 50 × 50 nm^2.

arrangement of the molecules in the row structure undetermined.

2.3 Gradual ordering and stability of the scan-ordered phase

The scan-induced ordering of $PyC_{12}SH$ SAM was investigated step by step for its mechanism and stability. Fig. 3a was obtained after 20 min of scans with a relatively less invasive scan condition (I_t = 50 pA, V_{tip} = −0.8 V). The STM topography in this phase was characterized by randomly distributed small corrugations with lateral sizes smaller than a few nm. After this area was scanned with I_t = 500 pA and V_{tip} = 1.0 V, molecular row patterns suddenly appeared. However, the characteristic three-fold rotational symmetry seen in Fig. 2b was not evident at this stage (the encircled area of Fig. 3b). We assume that at this stage, the scanned area was in its intermediately ordered phase, where the S–Au head parts of the $PyC_{12}S$ molecules were not yet periodically arranged and ordered in registry with the underlying Au(111) substrate. After an additional 10 min of scans, the molecules became ordered better, perhaps commensurable with the substrate. The row structures in the encircled area of Fig. 3c were evolved from the less-compliant rows of Fig. 3b to comply with the 120° rule imposed by the symmetry of the Au(111) substrate. Through these processes, Au vacancy coarsening occurred to a lesser extent than that in Fig. 2b, presumably due to less invasive scan conditions.

The same area was scanned after being left for 12 h to check the stability of the scan-ordered phase (Fig. 3d). Au vacancy coarsening occurred to a large extent in this area. A similar phenomenon for dodecanethiol SAMs has been previously reported and attributed to a relaxation of residual stress induced in the system upon scanning.[23] The row structures seen in Fig. 3c were also disrupted by this relaxation process, leading to random cluster-like structures, such as those seen in Fig. 3a. However, this observation did not suffice to conclude that the ordered phase was metastable, because this disruption of row structures was accompanied or driven by the Au sublayer relaxation. After these processes, the area was scanned with a positive tip bias, and then imaged with a negative tip bias. This scanning with a positive tip bias caused the row structures to be re-formed (Fig. 3e). It is evident that the formation of row structures did not prevent the SAM from being relaxed and reorganized. Therefore, any interpretation

of the row structure formation with possible polymerization of pyrrolyl endgroups could be definitely excluded.

We found that negative tip biases gave crisper and more stable images, while positive tip biases gave quicker ordering. This phenomenon may indicate that electronic or electrostatic contribution was considerable in the scan-induced ordering process. The influence of tip bias polarity on the stability of alkanethiol SAMs has been discussed by Yang and Liu.[5] In the report, desorption of the molecules from the SAMs was observed at large negative tip biases, while no desorption was observed at positive tip biases. It has been argued that negative tip biases tend to weaken the Au–S bonds *via* field-induced charge redistribution. This property has been inversely utilized by many experimenters: positively pulsed tip biases have been used for *in situ* tip cleaning on alkanethiol SAMs. However, $PyC_{12}SH$ SAMs showed a different property: negative tip bias pulses gave better results in tip cleaning, while scanning with positive tip biases tended to contaminate the tip.

It is possible that this polarity-reversed response was caused by a difference in molecular dipole moments.[25] If this was the case, weakening of Au–S bonds might not be the reason for the facile rearrangements in the $PyC_{12}SH$ SAM by positive tip biases. Additionally, it is also possible that packing of pyrrolyl endgroups was promoted by positive tip biases. With a positively biased tip engaged, pyrrolyl moieties near the tip would become more negatively charged. Delocalization of this excess negative charge may be facilitated by close-packing of the pyrrolyl moieties, thus lowering the overall system energy. The appearance of molecular row structures, which did not follow the symmetry of Au(111) substrate (in Fig. 3b), may imply the importance of pyrrolyl endgroup packing as a driving force of the ordering. Finally, it is hardly probable that the difference in the ordering efficiency caused by tip bias polarity change resulted from a difference in relative tip heights. Although typically measured I–V_{tip} curves on $PyC_{12}SH$ SAMs were asymmetric, which indicated that the magnitude of tunneling current was changed with tip bias polarity, the difference was not substantial to make a significant change in tip height.

2.4 Odd–even effect in scan-induced ordering

The scan-induced ordering effect was also observed in $PyC_{11}SH$ SAM, which was also in a disordered phase when assembled at RT. After being stimulated by repetitive STM scans, the SAM became ordered as shown in Fig. 4. All characteristics of the ordered $PyC_{11}SH$ SAM, such as the inter-row corrugation period, were similar to those of the scan-ordered $PyC_{12}SH$ SAM.

Distinguished odd–even effects have been observed in many alkanethiol SAM systems on Au(111) with phenyl-based endgroups.[3,5–8,26] It is well known that phenyl- or methylbiphenyl-terminated SAMs with odd numbers of methylene linkers (PhC_nSH or BPn SAMs with odd n) form $(\sqrt{3}\times2\sqrt{3})R30°$-based structures with the aromatic endgroups packed in a herringbone fashion. For even n, this endgroup packing is hindered as the tilt angle of the aromatic rings from surface normal increases due to a fixed bonding geometry of the thiol

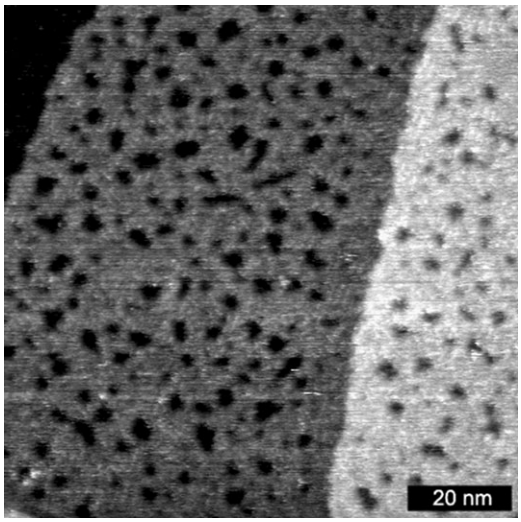

Fig. 4 An STM topograph of $PyC_{11}SH$ SAM ordered by scanning for 10 min with I_t = 30 pA and V_{tip} = 0.4 V. (Imaging conditions: I_t = 30 pA and V_{tip} = 0.874 V).

headgroups (the S–C bonds being sp^3-hybridized). Therefore, the SAMs are formed in various molecular arrangement structures with larger unit cells. While a striking variety of SAM structures has been obtained in those systems with shorter alkyl linker lengths, such a variation in SAM structures was not observed in atomic force microscopy (AFM) measurements of PhC_nSH SAMs with long alkyl linkers ($n \geq 12$).[3] This is thought to be caused by an enhanced stress relaxation *via* long alkyl linkers, which may enable a herringbone packing among the phenyl endgroups irrespective of the number of methylene linkers being odd or even. The same explanation may be applied to this PyC_nSH SAM system. The absence of odd–even effect in scan-induced ordering of PyC_nSH SAMs might imply that (1) the row structure in the ordered phase was largely determined by an ordering between the pyrrolyl endgroups as the hexagonal structure in PhC_nSH SAMs was determined by the herringbone ordering between the phenyl groups,[27] and (2) the PyC_nS molecules (with either odd or even n) adapted themselves for the packing of the pyrrolyl endgroups into the row structure, possibly *via* some deformation within the alkyl chain linkers.

2.5 Ordering by thermal annealing at 70 °C

After being annealed at a higher temperature (~70 °C), the $PyC_{12}SH$ SAM turned into a quasi-ordered phase (Fig. 5a). The corrugation period of the row structure was measured to be 1.47 ± 0.07 nm. Symmetry of the domain orientations was also the same as that of the scan-ordered phase. Therefore, we conclude that this ordered phase in thermally annealed SAM (HT-SAM) had the same molecular arrangement as the scan-ordered phase.

Although average domain size in the HT-SAM was larger than that of the scan-ordered phase shown in Fig. 2b, there still were many defects in each domain. These defects included discontinuities in row structures and dislocations in some of the parallel rows, implying that the commensurability between the ordered rows of the pyrrolyl endgroups and the Au–S

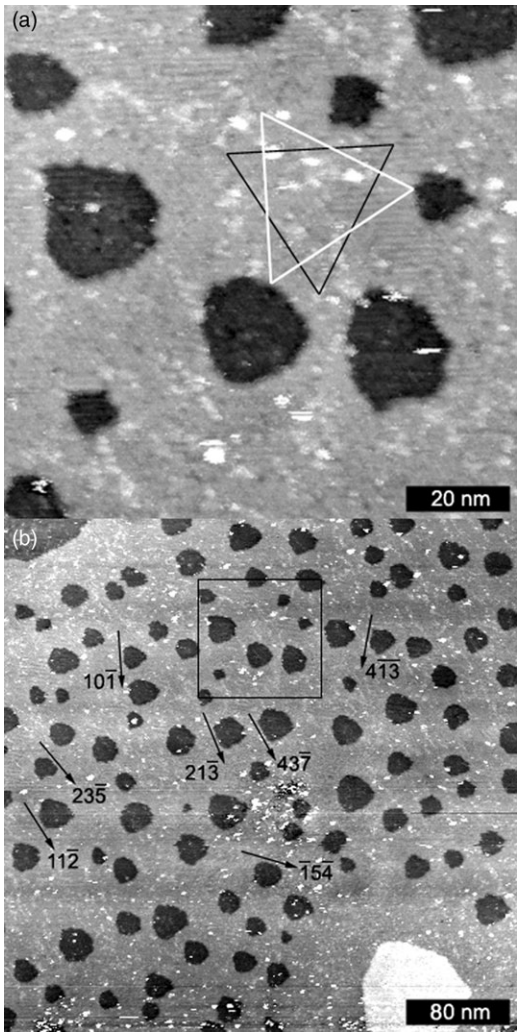

Fig. 5 STM topographs of $PyC_{12}SH$ SAM annealed at 70 °C. (a) A close-up scan image from the boxed area of (b). Triangles with edges parallel to NNN (black) or NN (white) directions of the Au(111) substrate were drawn as guides. The scanned area is 100 × 100 nm^2. (b) A large scale image from an area of 400 × 400 nm^2. Most of the coalesced etch pits had rounded-off polygonal shapes with edges parallel to surface vectors with small indices on Au(111). Some of the edge directions were indicated by indexed arrows. Images were taken with I_t = 20 pA, V_{tip} = −1.0 V.

headgroup parts was not perfect, and thus a stress, which was high enough to limit the molecular row length to ≤10 nm, was developed along the row direction. There were also small areas of indefinite shapes that appeared to be higher than the ordered area. These areas were thought to be covered by molecules that had smaller tilt angles and larger lateral molecular densities than those in the ordered area. The degree of long range order or the integrity of molecular arrangement in the ordered phase did not appear to affect the free energy of the system significantly.

As a result of Ostwald ripening process during the thermal annealing,[7,28] the Au vacancies coalesced into larger ones with a lower number density compared to that of the RT-SAM (Fig. 5b). The coalesced etch pits mostly had rounded-off polygonal shapes, with edges parallel to various surface vectors with small indices on Au(111). Some of the surface vectors were indicated in Fig. 5b. It was often observed that etch pits in thiol SAMs on Au(111) with $(\sqrt{3}\times\sqrt{3})R30°$-based structures had hexagonal (or triangular) shapes with edges parallel to the $\langle 11\bar{2}\rangle$[8,9] or $\langle 1\bar{1}0\rangle$[29] directional sets which were shown by the black and the white triangle in Fig. 5a, respectively. Since the two directional sets correspond to NN directions of the molecules and of the top Au atoms, such directional formation of step boundaries should contribute to minimize the system energy, depending on the relative strength of intermolecular interactions to that of interatomic interactions in the substrate. However, coalesced etch pits in the HT-SAM of $PyC_{12}SH$ did not show such a preference in edge directions. This observation indicates that the ordered structure was not a $(\sqrt{3}\times\sqrt{3})R30°$-based one, and/or the ordered phase had such a high defect density that faceting in some preferential directions would not give even a marginal reduction in the system energy.

The corrugation height of molecular rows in this ordered phase was measured to be about 0.07 nm under the scan conditions. This corrugation height is typical for ordered thiol SAMs terminated by aromatic moieties.[6,30] There have been reports of corrugations of similar magnitudes (0.05–0.1 nm) in superstructures of ordered phases of $H_3C–C_6H_4–C_6H_4–(CH_2)_n–SH$ (BP*n*) SAMs on Au(111).[7,8] In these systems, each of the ordered phases had a superstructure that was superimposed over a simpler base structure, and the molecular packings inside lower features turned out to be the same as those in higher features of the superstructures. The periodic topographic features in STM images were explained to be caused by a small mismatch between ideal lattice dimensions for the BP*n* monolayers and the underlying Au substrate. In other words, the superstructures were attributed to S atoms being adsorbed at different sites on Au substrates. The authors also acknowledged possible reconstructions in the Au top layer, which may contribute to lower the overall system energy. The same explanations might be applicable to the ordered phase of $PyC_{12}SH$ SAM.

2.6 Molecular coverage of $PyC_{12}SH$ SAM

The molecular coverages of $PyC_{12}SH$ RT- and HT-SAMs were measured by cyclic voltammetry (CV). A series of successive voltammetric scans for the HT-SAM is given in Fig. 6. An irreversible anodic peak was observed near the electrode potential of 0.8 V, which was attributed to oxidation of pyrrolyl units in the SAM.[11–14] No polymeric wave could be seen in voltammetry cycles subsequent to the first cycle, probably because no special efforts were carried out to remove residual water from the electrolyte solution.[11] Because neither polymeric wave nor pyrrolyl monomer oxidation[31] prior to the CV scans was detected, the number of molecules in the CV-active area could be counted by a ratio of $2e^-$ per molecule,[12,13] using the shaded area in Fig. 6 as the total charge transferred from the pyrrolyl units. The average surface molecular densities of RT- and HT-SAMs were calculated to be $(6.0 \pm 0.2)\times10^{-10}$ and $(5.9 \pm 0.2)\times10^{-10}$ mol cm^{-2}, respectively. These values corresponded to ~77% of the experimental alkanethiol SAM coverage (7.8×10^{-10} mol

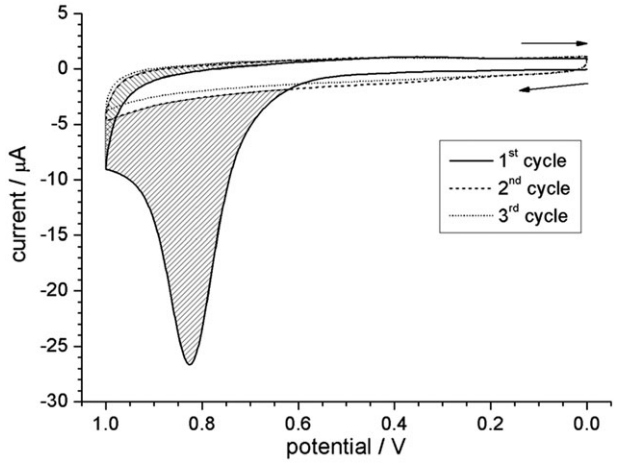

Fig. 6 Cyclic voltammograms obtained with a scan rate of 0.1 V s^{-1} from Au electrode surfaces covered by $PyC_{12}SH$ SAM annealed at 70 °C. The shaded area corresponds to the oxidation peak area of pyrrolyl units in the SAM.

cm^{-2}, which is compatible with the $(\sqrt{3}\times\sqrt{3})R30°$-based close-packing),[32] and there was no appreciable difference in molecular coverage between RT- and HT-SAM of $PyC_{12}SH$.

We crosschecked the molecular coverage of the $PyC_{12}SH$ SAMs by using XPS. It has been well established that photoelectron intensity from Au substrates covered with alkanethiol SAMs decreases logarithmically with increasing the alkyl chain length.[33] Effective thicknesses of the SAMs were estimated by comparing the attenuation of Au 4f XPS signals with those from a reference system of simple alkanethiol SAMs (C_nSH SAM, with n = 10, 12, 15, 16, 18). The least-squares fit from the reference system was used to determine the effective thicknesses and lateral packing densities of the $PyC_{12}SH$ SAMs (Fig. 7). The effective thicknesses of the RT- and HT-SAMs of $PyC_{12}SH$ were determined to be equivalent to those of $C_{12.5}SH$ and $C_{12.4}SH$, respectively. From these values, the lateral packing densities of $PyC_{12}S$ molecules in RT- and HT-SAMs were calculated to be 79.7 and 78.9% of the alkanethiol reference system, respectively.[34] This molecular coverage of ~79% agreed well with the value of ~77% obtained from the CV measurements within experimental error.

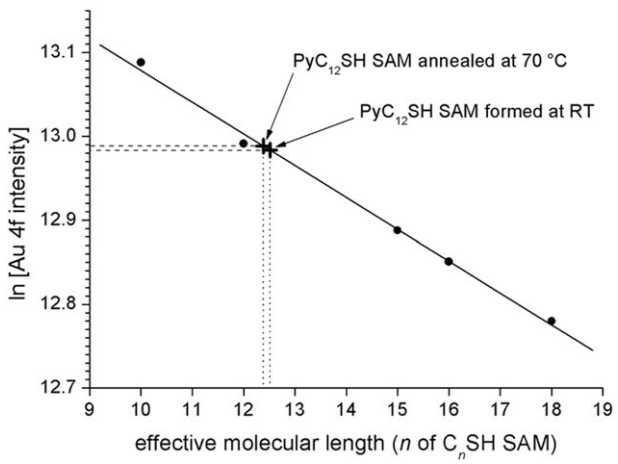

Fig. 7 Attenuation of the substrate photoelectron intensity (Au 4f) of the $PyC_{12}SH$ SAMs. Values from simple alkanethiol SAMs (C_nSH SAMs, n = 10, 12, 15, 16, 18) were used to obtain effective molecular lengths of the $PyC_{12}SH$ SAMs. The effective molecular lengths were used to estimate surface molecular coverages of the SAMs.

2.7 Thickness of $PyC_{12}SH$ SAM

The thickness of the $PyC_{12}SH$ SAM was measured by ellipsometry. Ellipsometric measurements gave thicknesses t = 1.5 ± 0.03 nm for the RT-SAM, and t = 1.44 ± 0.04 nm for the HT-SAM. Compared to t = 1.78 nm of phenyl-terminated dodecanethiol ($PhC_{12}SH$) SAM, where the molecules are close-packed,[3] the thickness of the $PyC_{12}SH$ SAM corresponded to ~84% of that of $PhC_{12}SH$ SAM. Since there should be no substantial size difference between phenyl and pyrrolyl moieties, this difference in SAM thickness must be caused by a difference in lateral molecular densities, which again agrees with the previous results from CV and XPS.

We have also tried to measure the thickness of the $PyC_{12}SH$ RT-SAM by scanning tunneling spectroscopy (STS). During STM scans with a relatively high impedance condition (I_t = 30 pA, V_{tip} = −1.0 V), tunneling currents with respect to tip height were obtained at arbitrary points on the sample. A typical tunneling current *versus* tip height (*I*–*z*) relation is shown in Fig. 8.[35] There was no kink in the linear fit of the data, indicating that the tip was in contact with the SAM within the range of $-0.5 \leq z \leq 0.2$ nm,[5] and the tip was partially penetrating or at least touching the SAM throughout the STM measurements in this work. At $z \geq 0.2$ nm, noisier datapoints could be seen which were caused by instrumental limitation in these measurements. Assuming tunneling resistance $R \approx 10$ kΩ for a mechanical contact between the tip and the gold substrate,[36] the SAM thickness was estimated to be ≥ 1.5 nm. However, this lower limit of the SAM thickness was probably overestimated, because SAM thicknesses measured by *I*–*z* STS tend to be larger than the true SAM thicknesses due to strong interactions between the biased tip and the molecules.[9]

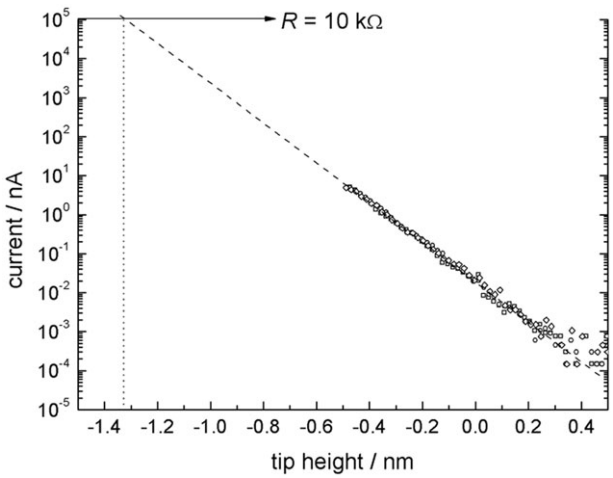

Fig. 8 Tunneling current *versus* tip height (*I*–*z*) of the $PyC_{12}SH$ RT-SAM. By a linear fit of log(*I*) *versus* *z*, the SAM thickness was estimated to be ≥ 1.5 nm. The feedback setpoint (I_t = 30 pA, V_{tip} = −1.0 V) was used for the reference tip height (z = 0).

The effective tunneling barrier height in I–z spectroscopy is given as $\Phi = -0.952[\Delta\ln(I)/\Delta z]^2$ (in eV and Å).[5] From the slopes of linear fits, a barrier height $\Phi = 1.31 \pm 0.07$ eV was obtained for the $PyC_{12}SH$ SAM. Compared with $\Phi = 1.39 \pm 0.01$ eV for long alkanethiol SAMs,[37] this value seemed reasonable, considering that the pyrrolyl endgroups may contribute to decrease the measured tunneling barrier height with a lower energy gap or by enhancing lateral charge hopping.

2.8 Crystallinity of $PyC_{12}SH$ SAM

We qualitatively analyzed the degree of packing and orientation of $PyC_{12}S$ molecules on the RT- and HT-SAMs through PIERS measurements (Fig. 9). It is well known that information on alkyl chain conformation and packing in alkanethiol SAMs can be deduced from the peak positions of the CH_2 stretching vibrations.[38] In the IR spectra, the peaks from the symmetric methylene stretching mode $\nu_s(CH_2)$ appeared at 2848 cm^{-1}, and those from the antisymmetric stretching mode $\nu_a(CH_2)$ appeared at 2918–2919 cm^{-1}. These values match with those from well-ordered and close-packed long alkanethiol SAMs.[38] In addition, it has been suggested that a frequency increase in these vibration modes may happen with reduced chain–chain interactions, even when the alkyl chains are in an all-*trans* conformation.[38] Therefore, it can be concluded that the alkyl chain parts in both the RT- and HT-SAMs of $PyC_{12}SH$ were not only in almost all-*trans* configurations, but also compactly packed with each other.

Since only the components of the vibrational transition dipole moments perpendicular to the surface plane contribute to the absorption spectra, the relative intensities of these methylene vibration peaks reveal additional information on twist angle of the alkyl chains.[3] The twist angle is defined as the rotation angle of the plane containing the –C–C–C– alkyl backbone with respect to the plane normal to the surface and containing the chain axis, on the assumption of an all-*trans* configuration. The transition dipole direction of the antisymmetric mode is orthogonal to the backbone plane, and that of the symmetric mode is parallel to the backbone plane and normal to the chain axis. Although both of the mode intensities depend on the chain tilt angle as well as on the twist angle, we can safely assume that there is no substantial difference in the chain tilt angle between the RT- and HT-SAMs, based on the results that the molecular coverages and thicknesses showed no substantial difference between the RT- and HT-SAMs. The ratios of peak areas $\nu_s(CH_2)/\nu_a(CH_2)$ were 0.51 and 0.28 for the RT- and HT-SAMs, respectively. These ratios indicate that the average twist angle of the HT-SAM was larger (closer to $\pm 90°$) than that of the RT-SAM.

This result was analogous to the results of Lee *et al.*, in which larger twist angles were obtained for PhC_nSH SAMs with even n, and smaller twist angles for odd n.[3] The authors attributed this phenomenon to different degrees of interactions of terminal phenyl group in odd- *versus* even-numbered films, which resulted from different tilt angles of the terminal phenyl groups (larger tilt angles for n = even). In other words, twist angles of the alkane chains in PhC_nSH SAMs with even n should be larger compared to the SAMs with odd n, to accomodate terminal phenyl groups into an ordered state by reducing their vertically projected size. The major difference between our results and those from PhC_nSH SAMs is that in our results, the twist angle change came only from thermal annealing, which was not accompanied by an appreciable change in the surface molecular coverage.

Spectral intensities of vibrational modes in the pyrrolyl endgroups were also compared between RT- and HT-SAMs for orientational information in a similar way. In the range of 900–1600 cm^{-1}, three absorption peaks were well discriminated from the background: two of them were from in-plane modes ν(C=C) and δ(C–H), and one from ν(C–N),[13] which was assumed to be also in the ring plane by sp^2-hybridization of the N atom. All three peaks from the HT-SAM were smaller than those from the RT-SAM, indicating that the pyrrole rings in the HT-SAM were oriented more parallel to the substrate on average. This result may seem contradictory to the result that the average twist angle of the alkyl backbones in the HT-SAM was larger than that of the RT-SAM. This contradiction could be resolved if it is assumed that there are some

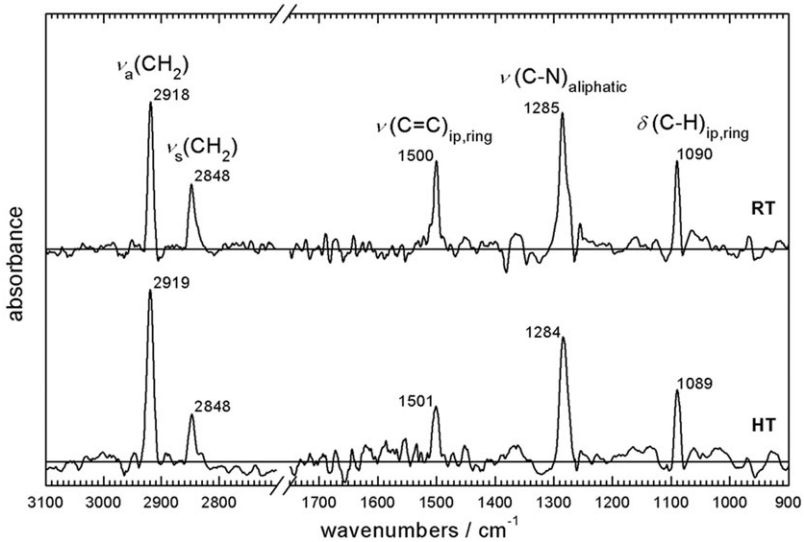

Fig. 9 PIERS spectra of the RT- and HT-SAMs of $PyC_{12}SH$.

gauche defects near the pyrrolyl endgroups in the RT-SAM or some of the thiols in the RT-SAM are bonded to the Au substrate with a twist angle near 180° (*via* sp-hybridization or different adsorption sites),[39,40] allowing the pyrrole rings in the RT-SAM to be more upright than those in the HT-SAM without affecting the infrared spectral properties of the alkyl chains (as shown in Fig. 10a). This model also explains the disordered nature of RT-SAM of $PyC_{12}SH$ observed by STM (Table 1).

We verified the orientational properties of the pyrrolyl endgroups in the $PyC_{12}SH$ SAMs *via* contact angle measurements. For all of the three probe liquids used (dimethyl formamide, methylene iodide, and nitrobenzene), contact angles were lower on the HT-SAM than on the RT-SAM of $PyC_{12}SH$. This trend was also consistent with the results of Lee *et al.*,[3] in which advancing contact angles of the probe liquids on PhC_nSH SAMs were shown to be lower for even n than for odd n, probably due to a larger tilt angle of the terminal phenyl groups in the SAMs with even n. Therefore, this result supports the observation that the pyrrole rings in the HT-SAM were oriented more parallel to the substrate with larger tilt angles than those in the RT-SAM.

2.9 Ordered phase of $PyC_{12}SH$ SAM

Although molecularly resolved STM images could not be obtained for the ordered $PyC_{12}SH$ SAM, a feasible molecular structure could be proposed based on the coverage, thickness, and orientational properties obtained for the SAM. The row structure in the ordered $PyC_{12}SH$ SAM bore a superficial resemblance with the AFM scan-induced $p(3\times1)$ superstructure observed in decanethiol SAM.[18] However, there was a difference in the corrugation period between the $p(3\times1)$ phase and the ordered phase of the $PyC_{12}SH$ SAM (1.33 nm for the $p(3\times1)$ superlattice of $(\sqrt{3}\times\sqrt{3})R30°$ structure), let alone the difference in surface molecular coverage.

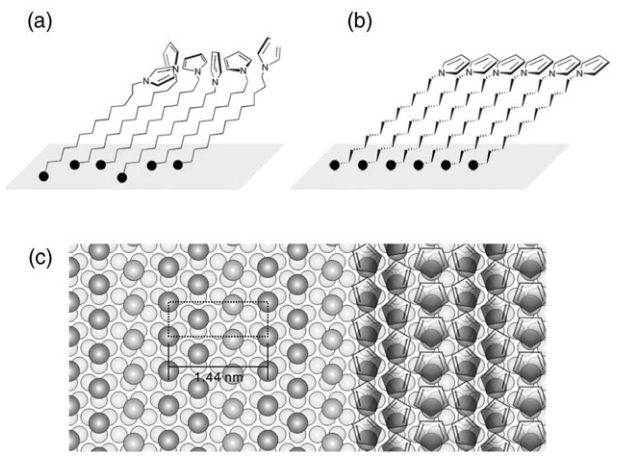

Fig. 10 Schematic drawings of the $PyC_{12}SH$ SAMs: (a) disordered RT-SAM, and (b) ordered SAM. The alkyl chains in both SAMs are thought to be closely packed, although the substrate–molecule registry might be different. (c) The proposed structure of the ordered PyC_nSH SAM ($(5\times\sqrt{3})$rect phase). Small circles represent top layer Au atoms. A hypothetical arrangement between the pyrrolyl endgroups is illustrated on the right side of the drawing. Choice of S–Au adsorption sites is arbitrary, and possible substrate reconstructions are not considered in the drawing.

Table 1 Static contact angles (θ_s) of dimethyl formamide (DMF), methylene iodide (MI), and nitrobenzene (NB) on the $PyC_{12}SH$ SAMs

	θ_s (DMF)	θ_s (MI)	θ_s (NB)
$PyC_{12}SH$-RT	39.3 ± 1.4°	33.7 ± 1.1°	21.1 ± 0.9°
$PyC_{12}SH$-HT	38.7 ± 1.5°	30.7 ± 1.2°	16.2 ± 0.9°

From the fact that the $PyC_{12}SH$ HT-SAM had a molecular coverage of $\geq 77\%$ of the close-packed alkanethiol SAMs while having a compactly-packed alkyl linker layer, it can be deduced that the tilt angle of the $PyC_{12}S$ was larger than that of the close-packed alkanethiol SAMs. Barrena *et al.* have reported various below-saturation phases of alkanethiol SAMs that have larger molecular tilt angles than ~35° of the $(\sqrt{3}\times\sqrt{3})R30°$-based structures.[19] Among them, $(2\times\sqrt{3})$rect and $(4\times\sqrt{3})$rect phases with a tilt angle of ~50° had a surface molecular coverage of 75% with respect to that of saturated $(\sqrt{3}\times\sqrt{3})R30°$-based structures. A (2×2)-based structure with the same 75% coverage also has been predicted for alkanethiol SAM systems by a chain-interlocking model,[21] which was not observed experimentally.[20] These structures or their variants could be possible candidates for the Au–S registry of the ordered $PyC_{12}SH$ SAM. However, although the molecular coverage of these models is close to the experimental values for the ordered $PyC_{12}SH$ SAM, these structural models are not quite compatible with the row structure along $\langle 11\bar{2}\rangle$ directions with a corrugation period of ~1.47 nm.

Fig. 10c shows a $(5\times\sqrt{3})$rect structure on Au(111) that has a row corrugation period of 1.44 nm and a surface molecular coverage of 90% of the close-packed alkanethiol SAMs. This structure has row directions parallel to the $\langle 11\bar{2}\rangle$ directional set and its row corrugation period is similar to the experimental value, 1.47 ± 0.07 nm. We propose that the ordered $PyC_{12}SH$ SAM has a molecular arrangement based on this structure. The disparity in surface molecular coverages obtained from the experiments (~77–79%) and of the model (90%) can be attributed to molecular defects which are thought to be manifested in the ordered $PyC_{12}SH$ SAM shown in Fig. 5a. A similar molecular row pattern has been reported to occur in microcontact-printed dodecanethiol SAMs on Au(111) by Larsen *et al.*[10] The authors assumed this phase to have a $(5\times\sqrt{3})$rect structure with 2 molecules per unit cell. However, this assignment of the surface molecular density (60%) had not been firmly based on observations.

In a recent molecular dynamics simulation, the liquid state of pyrrole has been described as a complex aggregate of pyrrole dimers oscillating between hydrogen-bonded T-shapes and π-bonded stacked forms.[41] This report may imply that a near parallel-displaced arrangement between pyrrolyl groups can be one of possible structural features in the ordered phase of the $PyC_{12}SH$ SAM, in addition to the usual herringbone-like arrangement between small aromatic moieties such as phenyl or biphenyl groups. A hypothetical arrangement between the pyrrolyl endgroups is drawn in Fig. 10c, which pertain to those structural elements aforementioned: herringbone-like and parallel-displaced arrangements between the pyrrolyl endgroups that are heavily tilted from the surface

normal. In a recent study of 9-mercaptoanthracene SAM on Au(111), a distance of ~0.56 nm between π–π near-parallel-displaced anthryl groups has been reported.[42] In the proposed $(5\times\sqrt{3})$rect structure, intermolecular distance along the row direction should be the NNN distance of Au(111), which is 0.4995 nm. This mismatch in the intermolecular distance may be the source of stress, which is thought to have caused the molecular defects in the ordered phase of the PyC_nSH SAM.

2.10 Disorder and order in PyC_nSH SAMs

The ordering in PyC_nSH SAMs had similar aspects to the $(\sqrt{3}\times\sqrt{3})R30^\circ \rightarrow c(4\times2)$ superlattice transformation observed in decanethiol SAM on Au(111).[18] It can be induced by both STM scan and thermal annealing, and causes a change in the average twist angle of the alkane chains, while not causing a practical change in lateral molecular coverage. There also have been other reports of phase transformations in thiol SAM systems on Au(111) which are induced by thermal annealing or scanning probes (with STM or AFM).[8,19–21] For example, Cyganik and Buck have reported a thermally induced irreversible phase transformation in BP4 SAM on Au(111).[4] In this system, the SAM, initially in a $(5\sqrt{3}\times3)$rect phase with an area per molecule of 27 $Å^2$ (α-phase) at room temperature, was transformed into a $(6\sqrt{3}\times2\sqrt{3})$oblique phase with an area per molecule of 32.4 $Å^2$ (β-phase), which was less dense and more stable, after annealing at 373 K. They attributed this phenomenon to an energy hyperspace which had a number of pronounced local minima caused by a competition between different factors contributing to the total energy of the system. Factors such as Au–S–C bonding geometry, molecular adsorption sites, interaction between alkyl chains, and interactions between aromatic endgroups (such as π-stacking, steric repulsion, and dipole interaction) were thought to determine the energy hyperspace. The major difference between the ordering in PyC_nSH SAMs and the phase transformations in decanethiol and BP4 SAMs was that the PyC_nSH SAMs were formed in a disordered phase at RT, whereas the other SAMs were already in ordered phases at RT.

To date, there has not been any report of disorder–order phase transformation in molecular SAM systems. We suspect that this special characteristic of PyC_nSH SAMs is caused by a much stronger and complex interaction between the pyrrolyl endgroups that have a heterogeneity within the aromatic ring: the N atom. The disordered nature of the SAMs at RT may be caused by a dipole–dipole interaction between the pyrrolyl groups that disturbs an orderly packing of the endgroups and imposes a high energy barrier to the ordered phase. As was mentioned previously, PyC_nSH molecules with $n \leq 10$ also form disordered SAMs. On the contrary, it is known that PhC_nSH SAMs with odd n are ordered *via* a herringbone arrangement of phenyl endgroups in the $(\sqrt{3}\times2\sqrt{3})R30^\circ$ structure.[3,5] It is quite noteworthy that a small difference in the aromatic endgroups (phenyl *versus* pyrrolyl) leads to such a change in molecular arrangement.[43]

Pyrrole molecules are known to form N–H$\cdots\pi$ hydrogen bonds readily with each other.[44,45] Although such an intermolecular bonding is decapacitated in the alkanethiol-derivatized PyC_nSH molecules, it is highly probable that an inherent strong dipole of the pyrrolyl group still disturbs the usual herringbone packing between aromatic moieties,[46,47] yielding disordered SAMs for these molecules. This dipole-induced disorder seems to persist even in the $PyC_{12}SH$ RT-SAM, which was shown to have a compactly packed alkyl linker layer by the PIERS analysis and a higher surface molecular coverage by the CV and XPS analyses, in contrast to PyC_nSH SAMs with smaller n. As was suggested in section 2.8, this disorder is probably enabled by gauche defects near the pyrrolyl endgroups as depicted in Fig. 10a. A parallel-shifted packing between pyrrolyl groups such as shown in Fig. 10b may help to relieve the destabilizing dipole–dipole interaction, which is probably the main reason for the disorder in RT-SAMs of PyC_nSH. Such endgroup packing also conforms to the molecular orientational properties deduced from the PIERS data.

It seems highly probable that kinetic factors rather than thermodynamic ones determine the phase of the RT-SAMs. However, although only an insignificant difference in surface molecular coverage was found between the RT- and HT-SAM, this did not necessarily mean that surface molecular densities were identical between the ordered and the disordered phases. Strictly speaking, the HT-SAM consisted of two different phases: the ordered phase, and a disordered phase which had a higher surface molecular density than that of the ordered phase, as judged by higher STM heights of small disordered areas in Fig. 5a. This means that surface molecular density of the disordered phase may be slightly higher than that of the ordered phase. Therefore, it is possible that the disordered state was not just a kinetically limited state, but a thermodynamically favored one over the ordered state at RT in terms of total enthalpy of the self-assembly system.

As has been discussed by Touzov and Gorman,[18] mechanical interactions between scanning probe tips and samples are thought to be mostly responsible for scan-induced phase changes observed in many thiol SAM systems. The same mechanism must be also responsible for the scan-induced ordering in this work, because the STM tips partially penetrate into the SAM under the scan conditions used here. The mechanical agitation exercised by the STM tips must have helped the disordered PyC_nS molecules to overcome the energy barrier to the ordered phase. However, as was discussed in the previous section, contributions from electrostatic and/or electronic interactions between the tip and the PyC_nS molecules may also be considerable. In addition, there might be another factor which was related to the bias polarity-dependent ordering efficiency: transfer of PyC_nS molecules from the SAMs to the tip. As was stated earlier, the disordered RT-SAM is thought to have a slightly higher surface molecular density than the ordered phase. It is possible that molecular transfer from the SAM to the tip, which was enhanced at positive tip biases, had accelerated the ordering process.

3. Experimental

Materials

Pyrrole (98%, Aldrich), 1,11-dibromoundecane (98 + %, Aldrich), 1,12-dibromododecane (98%, Aldrich), thiourea

(99%, Sigma–Aldrich), potassium hydroxide (KOH, 85%, Junsei), sodium hydroxide (97%, Sigma–Aldrich), hydrochloric acid (HCl, 35%, Junsei), 1-decanethiol (96%, Aldrich), 1-dodecanethiol (98 + %, Aldrich), 1-pentadecanethiol (98%, Aldrich), 1-hexadecanethiol (95%, Fluka), 1-octadecanethiol (98%, Aldrich), tetrabutylammonium perchlorate (99%, Fluka), absolute ethanol (EtOH, 99.8 + %, Merck), dichloromethane (CH_2Cl_2, 100.0%, J. T. Baker, HPLC grade), anhydrous *N*,*N*-dimethylformamide (DMF, 99.8%, Sigma–Aldrich), methylene iodide (99%, Sigma–Aldrich), nitrobenzene (99 + %, Sigma–Aldrich), anhydrous acetonitrile (99.8%, Sigma–Aldrich) were used as received. Ultrapure water (18.3 MΩ cm) from Human Ultra Pure System (Human Corp., Korea) was used. Au/mica substrates were purchased from Agilent Technologies AFM (Arizona, USA), and Au/Cr/glass substrates were purchased from Arrandee (Germany).

Synthesis of molecules for the SAMs

12-(1*H*-Pyrrol-1-yl)dodecane-1-thiol ($PyC_{12}SH$) and 11-(1*H*-pyrrol-1-yl)undecane-1-thiol ($PyC_{11}SH$) were synthesized following the reported procedure.[14,15] In brief, pyrrole (5.7 mmol) and KOH (6.5 mmol) were added to anhydrous DMF solution (40 mL) containing 1,12-dibromododecane or 1,11-dibromoundecane (16 mmol), and the mixture was stirred to react at room temperature overnight. The reaction product was extracted with diethyl ether after addition of water (40 mL). After drying with $MgSO_4$, concentration of the product *in vacuo* followed by column chromatography provided 1-(12-bromododecyl)-1*H*-pyrrole (47% yield) or 1-(11-bromoundecyl)-1*H*-pyrrole (44% yield) as a pale yellow liquid. The synthesized compound (2.0 mmol) was mixed with thiourea (6 mmol) in ethanol (50 mL) and the solution was heated to reflux for 8 h. The reaction product was allowed to cool down to room temperature under an Ar purge, and then NaOH solution (4 mL, 10% w/w) was added to the product. The solution was heated to reflux for 4 h. Upon cooling to room temperature, the hydrolyzed solution was titrated with dilute HCl to pH 7. After extraction with diethyl ether, the organic phase was rinsed with water, dried with $MgSO_4$, and then purified by column chromatography to give $PyC_{11}SH$ (80% yield) and $PyC_{12}SH$ (76% yield) as a pale yellow liquid. ^1H NMR (300 MHz, $CDCl_3$): $PyC_{11}SH$, δ 1.27 (m, 15H), 1.66 (m, 2H), 1.76 (m, 2H), 2.53 (q, 2H), 3.86 (t, 2H), 6.14 (t, 2H), 6.65 (t, 2H); $PyC_{11}SH$, δ 1.27 (m, 15H), 1.64 (m, 2H), 1.76 (m, 2H), 2.53 (q, 2H), 3.87 (t, 2H), 6.14 (t, 2H), 6.65 (t, 2H). MS(EI) for $C_{15}H_{27}NS$ ($PyC_{11}SH$): calcd 253.1864, found 253.1512. MS(EI) for $C_{16}H_{29}NS$ ($PyC_{12}SH$): calcd 267.2021, found 267.1428.

Preparation of the SAMs

The SAMs of PyC_nSH (n = 11, 12) were formed on Au/mica, Au/Cr/glass (for STM measurements), or Au/Cr/Si substrates (for other measurements). The Au/Cr/glass substrates were hydrogen flame-annealed prior to the SAM formation. The SAMs were formed by immersing the gold substrates into ethanolic solutions (0.1 mM) of the thiol compounds under Ar atmosphere overnight at room temperature (RT).[48] Thermal annealing of $PyC_{12}SH$ SAM was done by immersing the RT-formed samples in the same solution at 70 °C for an hour.[49] Afterwards, the solution temperature was gradually lowered to room temperature before the sample was taken out from the solution. After the incubation, the substrates were rinsed with pure ethanol, and dried with an Ar stream. All experiments were conducted with freshly prepared samples.

Scanning tunneling microscopy (STM)

All STM measurements were carried out under an ultra-high vacuum (UHV) using a UHV-VT-SPM from Omicron Nanotechnology GmbH (Germany). All STM images were obtained in constant current mode, and tip biases with respect to grounded samples were presented throughout. Electrochemically etched W tips were used in the experiment. To compensate for errors in determining lateral feature sizes in the STM topographies caused by non-proportionality in piezo motion of the scanner and by differences in tip length, a highly oriented pyrolytic graphite sample was measured using the same scan size and speed of the SAM sample measurements and analyzed as a calibration reference.

Cyclic voltammetry (CV)

Cyclic voltammograms were acquired using a BAS 100B (Bioanalytical Systems, Inc.). The three-electrode electrochemical cell consisted of a modified Au electrode, a Pt wire counter electrode, and an Ag/Ag^+ reference electrode. Experiments were carried out in degassed and anhydrous acetonitrile solution containing tetrabutylammonium perchlorate (0.1 M) as a carrier electrolyte. The active area of the gold electrode was 0.283 cm^2, and the surface coverage values were corrected for surface roughness, assuming a roughness factor of 1.2.[32,50]

X-Ray photoelectron spectroscopy (XPS)

The XPS spectra were obtained by using a VG-Scientific ESCALAB 250 spectrometer (UK) with a monochromatized Al Kα X-ray source (1486.6 eV) at an incidence angle of 58°. Emitted photoelectrons were detected by a multichannel detector at a takeoff angle of 90° relative to the surface. During the measurements, the base pressure was 10^{-9}–10^{-10} Torr. The lateral packing densities of the SAMs were calculated by investigating the attenuation of the Au 4f XPS signal. As a reference system, a series of SAMs of *n*-alkanethiols ($CH_3(CH_2)_{n-1}SH$, n = 10, 12, 15, 16, 18) on gold were used to determine the attenuation of the Au 4f signals as a function of effective molecular length.

Ellipsometry

The thicknesses of the monolayer films were measured with a Gaertner L116s ellipsometer (Gaertner Scientific Corp., IL, USA) equipped with a HeNe laser (632.8 nm) at a 70° angle of incidence. A refractive index of 1.46 was used for the films.

Polarized infrared external reflectance spectroscopy (PIERS)

The PIERS spectra were recorded with a nitrogen-purged Thermo Nicolet Fourier transform infrared spectrometer (model: NEXUS). The instrument was equipped with a liquid nitrogen-cooled mercury–cadmium–telluride (MCT) detector and a smart apertured grazing angle (Smart SAGA) apparatus

for grazing-angle reflectance IR spectroscopy. The *p*-polarized light was incident at 80° relative to the surface normal of the substrate. The spectra were taken by averaging approximately 2000 scans for background and 1000 scans for the samples (resolution of 2 cm^{-1}), and the final spectra were obtained with minimal baseline correction.

Contact angle measurement

Static contact angles were measured by using a Phoenix 300 goniometer (Surface Electro Optics Co., Ltd., Korea) at room temperature under ambient conditions. Dimethyl formamide, methylene iodide and nitrobenzene were used as probe liquids.

4. Conclusions

We studied structural phases of $PyC_{11}SH$ and $PyC_{12}SH$ SAMs on Au(111). By STM topographic measurements, the SAMs were found to be in a disordered phase when formed at room temperature. However, the PIERS results on the $PyC_{12}SH$ RT-SAM showed that the alkyl linker parts were in nearly all-*trans* configuration and compactly packed with each other. The PIERS data implied that the disorder was mostly confined to near-terminal parts of the molecules or to S–Au bonds, because of strong interchain interactions between the long alkyl linkers. The disorder was supposed to be caused by strong dipole–dipole interactions between the pyrrolyl endgroups.

The PyC_nSH SAMs underwent a disorder–order phase change by repetitive STM scans with invasive scan conditions. This scan-induced ordering was more facile with positive tip biases than with negative tip biases. We believe that electrostatic or electronic contributions to the ordering process were considerable, in addition to those from mechanical perturbation by the tip. It was found that the molecular ordering also could be accomplished by thermal annealing at 70 °C. The thermally ordered phase of the $PyC_{12}SH$ SAM had the same characteristics as the scan-ordered phase, such as a row corrugation period near 1.5 nm and abundance of defects. On the basis of the experimental results, the molecular arrangement in the ordered PyC_nSH SAM was proposed to be based on a $(5\times\sqrt{3})$rect structure.

There was practically no difference in surface molecular coverage between RT-formed and thermally ordered SAMs of $PyC_{12}SH$. From this result, it could be inferred that the disorder in the SAMs formed at RT should be ascribed to kinetic factors rather than thermodynamic ones. However, since it is possible that the disordered phase had a slightly higher surface molecular density than that of the ordered phase, the disordered state may be not only a kinetically limited state, but also a thermodynamically favored one over the ordered state at RT, in terms of total enthalpy of the self-assembly system.

The main focus of this work is on the effect of the dipolar pyrrolyl endgroups to the structural phases of the corresponding thiol SAM on gold. Our study not only filled in the current library of correlations between molecular species and their SAM structures, but also presented a novel instance of disorder–order phase transformation in molecular SAMs. We believe that this work can be beneficial for future studies to control structural properties of SAMs of various endgroups with diverse functionalities.

References

1 J. C. Love, L. A. Estroff, J. K. Kriebel, R. G. Nuzzo and G. M. Whitesides, *Chem. Rev.*, 2005, **105**, 1103.
2 C. Vericat, M. E. Vela and R. C. Salvarezza, *Phys. Chem. Chem. Phys.*, 2005, **7**, 3258.
3 S. Lee, A. Puck, M. Graupe, R. Colorado, Jr, Y.-S. Shon, T. R. Lee and S. S. Perry, *Langmuir*, 2001, **17**, 7364.
4 P. Cyganik and M. Buck, *J. Am. Chem. Soc.*, 2004, **126**, 5960.
5 G. Yang and G. Liu, *J. Phys. Chem. B*, 2003, **107**, 8746.
6 W. Azzam, P. Cyganik, G. Witte, M. Buck and C. Wöll, *Langmuir*, 2003, **19**, 8262.
7 P. Cyganic, M. Buck, W. Azzam and C. Wöll, *J. Phys. Chem. B*, 2004, **108**, 4989.
8 P. Cyganik, M. Buck, J. D. E. T. Wilton-Ely and C. Wöll, *J. Phys. Chem. B*, 2005, **109**, 10902.
9 G. J. Su, R. Aguilar-Sanchez, Z. Li, I. Pobelov, M. Homberger, U. Simon and T. Wandlowski, *ChemPhysChem*, 2007, **8**, 1037.
10 N. B. Larsen, H. Biebuyck, E. Delamarche and B. Michel, *J. Am. Chem. Soc.*, 1997, **119**, 3017.
11 R. J. Willicut and R. L. McCarley, *Anal. Chim. Acta*, 1995, **307**, 269.
12 R. J. Willicut and R. L. McCarley, *J. Am. Chem. Soc.*, 1994, **116**, 10823.
13 R. L. McCarley and R. J. Willicut, *J. Am. Chem. Soc.*, 1998, **120**, 9296.
14 R. J. Willicut and R. L. McCarley, *Langmuir*, 1995, **11**, 296.
15 C.-G. Wu, S.-C. Chiang and C.-H. Wu, *Langmuir*, 2002, **18**, 7473.
16 Y.-H. Kim, D. B. Wurm, M. W. Kim and Y.-T. Kim, *Thin Solid Films*, 1999, **352**, 138.
17 C. N. Sayre and D. M. Collard, *Langmuir*, 1995, **11**, 302.
18 I. Touzov and C. B. Gorman, *J. Phys. Chem. B*, 1997, **101**, 5263.
19 E. Barrena, E. Palacios-Lidón, C. Munuera, X. Torrelles, S. Ferrer, U. Jonas, M. Salmeron and C. Ocal, *J. Am. Chem. Soc.*, 2004, **126**, 385.
20 E. Barrena, C. Ocal and M. Salmeron, *J. Chem. Phys.*, 2001, **114**, 4210.
21 E. Barrena, C. Ocal and M. Salmeron, *J. Chem. Phys.*, 2000, **113**, 2413.
22 A. Kirakosian, M. J. Comstock, J. Cho and M. F. Crommie, *Phys. Rev. B: Condens. Matter Mater. Phys.*, 2005, **71**, 113409.
23 J. A. M. Sondag-Huethorst, C. Schönenberger and L. G. J. Fokkink, *J. Phys. Chem.*, 1994, **98**, 6826.
24 B. Lüssem, S. Karthäuser, H. Haselier and R. Waser, *Appl. Surf. Sci.*, 2005, **249**, 197.
25 The dipole moments of $C_{12}S$ and $PyC_{12}S$ radicals have been calculated to be 2.05 and −0.36 D from S heads to terminal groups, respectively. These values were obtained by density-functional calculations using B3PW91 with the 6-31G(*d*,*p*) basis set, after geometry optimizations of the respective free thiol molecules. We note that other methods such as *ab initio* calculations yielded similar values. Although these values do not truly represent partial charge distribution in the SAMs, they make a good basis for a qualitative comparison.For studies of dipole moments in thiol SAMs, see the following: I. H. Campbell, J. D. Kress, R. L. Martin, D. L. Smith, N. N. Barashkov and J. P. Ferraris, *Appl. Phys. Lett.*, 1997, **71**, 3528; R. W. Zehner, B. F. Parsons, R. P. Hsung and L. R. Sita, *Langmuir*, 1999, **15**, 1121. For the above calculations, the following software was used: M. J. Frisch, G. W. Trucks, H. B. Schlegel, G. E. Scuseria, M. A. Robb, J. R. Cheeseman, J. A. Montgomery, Jr., T. Vreven, K. N. Kudin, J. C. Burant, J. M. Millam, S. S. Iyengar, J. Tomasi, V. Barone, B. Mennucci, M. Cossi, G. Scalmani, N. Rega, G. A. Petersson, H. Nakatsuji, M. Hada, M. Ehara, K. Toyota, R. Fukuda, J. Hasegawa, M. Ishida, T. Nakajima, Y. Honda, O. Kitao, H. Nakai, M. Klene, X. Li, J. E. Knox, H. P. Hratchian, J. B. Cross, V. Bakken, C. Adamo, J. Jaramillo, R. Gomperts, R. E. Stratmann, O. Yazyev, A. J. Austin, R. Cammi, C. Pomelli, J. Ochterski, P. Y. Ayala, K. Morokuma, G. A. Voth, P. Salvador, J. J. Dannenberg, V. G. Zakrzewski, S. Dapprich, A. D. Daniels, M. C. Strain, O. Farkas, D. K. Malick, A. D. Rabuck, K. Raghavachari, J. B. Foresman,

J. V. Ortiz, Q. Cui, A. G. Baboul, S. Clifford, J. Cioslowski, B. B. Stefanov, G. Liu, A. Liashenko, P. Piskorz, I. Komaromi, R. L. Martin, D. J. Fox, T. Keith, M. A. Al-Laham, C. Y. Peng, A. Nanayakkara, M. Challacombe, P. M. W. Gill, B. G. Johnson, W. Chen, M. W. Wong, C. Gonzalez and J. A. Pople, *GAUSSIAN 03 (Revision B.03)*, Gaussian, Inc., Wallingford, CT, 2004.

26 T. Ishida, W. Mizutani, N. Choi, U. Akiba, M. Fujihira and H. Tokumoto, *J. Phys. Chem. B*, 2000, **104**, 11680.

27 H. H. Jung, Y. D. Won, S. Shin and K. Kim, *Langmuir*, 1999, **15**, 1147.

28 O. Cavalleri, A. Hirstein and K. Kern, *Surf. Sci.*, 1995, **340** L960.

29 J.-P. Bucher, L. Santesson and K. Kern, *Langmuir*, 1994, **10**, 979; J. Zhang, Q. Chi and J. Ulstrup, *Langmuir*, 2006, **22**, 6203.

30 G. Yang, Y. Qian, C. Engtrakul, L. R. Sita and G. Liu, *J. Phys. Chem. B*, 2000, **104**, 9059.

31 It is known that autoxidation of *N*-alkylpyrrole produces carbonyl-containing moieties such as succinimide. Since no carbonyl peak was observed near 1710 cm^{-1} in PIERS measurements of the $PyC_{12}SH$ SAMs (Fig. 9), the possibility of pyrrolyl autoxidation prior to the CV measurements could be excluded.

32 C. A. Widrig, C. Chung and M. D. Porter, *J. Electroanal. Chem.*, 1991, **310**, 335.

33 P. E. Laibinis, C. D. Bain and G. M. Whitesides, *J. Phys. Chem.*, 1991, **95**, 7017.

34 It has been reported that inelastic photoelectron scattering in surface layers of organic compounds can be predicted from the numbers of valence electrons, molecular densities, and bandgap energies of the compounds (S. Tanuma, C. J. Powell and D. R. Penn, *Surf. Interface Anal.*, 1993, **21**, 165). In this calculation, we assumed that the difference in the photoelectron attenuation between $PyC_{12}S$ and C_nS is solely governed by the number of valence electrons, n_{ve} (n_{ve} = 103 for $PyC_{12}S$, and $n_{ve} = (13 + 6n)$ for C_nS). For validity of this assumption, see the following: P. Harder, M. Grunze, R. Dahint, G. M. Whitesides and P. E. Laibinis, *J. Phys. Chem. B*, 1998, **102**, 426.

35 Since the samples frequently contaminated the tip while being scanned, the quality of STM image was constantly checked to exclude erroneous results due to tip contamination. Because contaminated tips or local contaminations on the surface would give noisier linear fits with less steep slopes or convexly curved fits, it could be assumed that these data were obtained with a clean tip.

36 J. K. Gimzewski and R. Möller, *Phys. Rev. B: Condens. Matter Mater. Phys.*, 1987, **36**, 1284.

37 W. Wang, T. Lee and M. A. Reed, *Phys. Rev. B: Condens. Matter Mater. Phys.*, 2003, **68**, 035416.

38 R. G. Nuzzo, F. A. Fusco and D. L. Allara, *J. Am. Chem. Soc.*, 1987, **109**, 2358.

39 C. Zeng, B. Li, B. Wang, H. Wang, K. Wang, J. Yang, J. G. Hou and Q. Zhu, *J. Chem. Phys.*, 2002, **117**, 851.

40 J. Nara, S. Higai, Y. Morikawa and T. Ohno, *J. Chem. Phys.*, 2004, **120**, 6705.

41 L. Gontrani, F. Ramondo and R. Caminiti, *Chem. Phys. Lett.*, 2006, **417**, 200.

42 R.-F. Dou, X.-C. Ma, L. Xi, H. L. Yip, K. Y. Wong, W. M. Lau, J.-F. Jia, Q.-K. Xue, W.-S. Yang, H. Ma and A. K.-Y. Jen, *Langmuir*, 2006, **22**, 3049.

43 Since the N atom in the pyrrolyl group is sp^2-hybridized as is C1 atom in the phenyl group, the molecular conformation of an isolated pyrrolyl-terminated alkanethiol is expected to be similar to that of a phenyl-terminated alkanethiol molecule.

44 A. Goméz-Zavaglia and R. Fausto, *J. Phys. Chem. A*, 2004, **108**, 6953.

45 R. Goddard, O. Heinemann and C. Krüger, *Acta Crystallogr., Sect. C: Cryst. Struct. Commun.*, 1997, **53**, 1846.

46 The influence of dipole–dipole or quadrupolar interactions between terminal groups on molecular ordering has been well demonstrated using a phenoxy-alkanethiol-based SAM system in the following work: Y.-Y. Luk, N. L. Abbott, J. N. Crain and F. J. Himpsel, *J. Chem. Phys.*, 2004, **120**, 10792.

47 The dipole moment of 1-methylpyrrole is ~2.13 D from aromatic ring to methyl group, while that of toluene is ~0.36 D. These values, obtained by density-functional calculations using B3PW91 with the 6-31G(*d*,*p*) basis set, were excerpted from the following: NIST Computational Chemistry Comparison and Benchmark Database, NIST Standard Reference Database Number 101 Release 12, Aug 2005, Editor: Russell D. Johnson III, http://srdata.nist.gov/cccbdb.

48 Usage of other solvents, such as toluene and DMF, resulted in the formation of small aggregates of the thiols physisorbed on the formed SAMs, which caused difficulties in STM measurements.

49 Increasing the annealing time also tended to intensify the contamination of the sample surface by the molecular aggregates, which was found to emerge even after a short annealing time of 1 h as shown in Fig. 5.

50 D. D. Popenoe, R. S. Deinhammer and M. D. Porter, *Langmuir*, 1992, **8**, 2521; S.-K. Oh, L. A. Baker and R. M. Crooks, *Langmuir*, 2002, **18**, 6981.